Journal of chemical & engineering data

Article

pubs.acs.org/jced

Storage of Methane in Clathrate Hydrates: Monte Carlo Simulations of sI Hydrates and Comparison with Experimental Measurements

Nikolaos I. Papadimitriou,[†] Ioannis N. Tsimpanogiannis,*[,†,‡] Ioannis G. Economou,*[,‡] and Athanassios K. Stubos[†]

[†]National Center for Scientific Research "Demokritos", Environmental Research Laboratory, 15310 Aghia Paraskevi Attikis, Greece

[‡]Texas A&M University at Qatar, Chemical Engineering Program, Education City, PO Box 23874, Doha, Qatar

Supporting Information

ABSTRACT: Extensive grand canonical Monte Carlo simulations are performed for the calculation of the amount of methane gas that can be stored inside the hydrate structure sI focusing on temperature and pressure conditions that are of interest to practical applications (e.g., methane storage/transportation, methane hydrates in nature). Langmuir-type "absorption isotherms" are used in order to present the results for methane in the cages of the hydrate structure. In particular, the methane content inside the different type of hydrate cages is given as a function of pressure, where the parameters of this function are temperature-dependent. A comparison between available experimental data for cage occupancies and calculated values resulted in good agreement. The correlation between chemical potential and pressure is determined through *NVT* Monte Carlo simulations. Simulations are performed for the TIP4P/Ice water model and two methane models (United−Atom and All−Atom). The calculations of the current study can be utilized during the process of refining the estimates of methane gas "in-place", in hydrate deposits, when pressure and temperature conditions at the hydrate reservoirs are known. A discussion on the implication to geologic media containing hydrates is also presented.

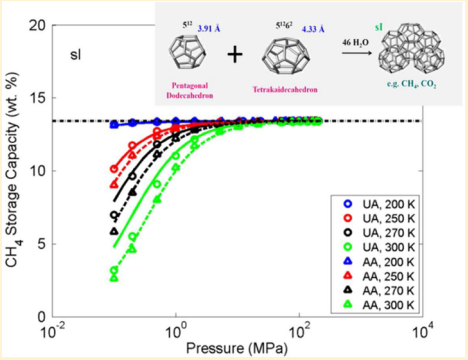

1. INTRODUCTION AND BACKGROUND

Conditions of high pressures or low temperatures in the presence of water, within natural or artificial environments, are suitable for the formation of nonstoichiometric, crystalline materials that are known as clathrate hydrates. The water molecules can form, through hydrogen-bonding, different types of cages/cavities that can be stabilized by the presence of guest molecules of particular sizes that can fit within the cages. Commonly encountered types of cages in hydrate-related studies include the following: pentagonal dodecahedron (5^{12}), tetrakaidecahedron ($5^{12}6^2$), hexakaidecahedron ($5^{12}6^4$), irregular dodecahedron ($4^35^66^3$), and icosahedron ($5^{12}6^8$). Different combinations of cage-types and cage-numbers can produce the building blocks (unit cells) for the three most common (i.e., sI, sII, and sH) hydrate structures.[1]

As a result of the discovery of large amounts of methane (CH_4) hydrates during the recent years in natural, geologic environments (e.g., inside oceanic sediments at the continental slopes, and at the Arctic permafrost regions), hydrates are currently considered possible future energy sources.[2−4] Preliminary estimates[5−7] of the total amount of CH_4 gas that is stored in hydrate deposits are encouraging and thus make the study of CH_4 hydrates very attractive, even though the total amount of stored CH_4 gas is still under debate within the scientific community.

On the other hand, the natural occurrence of CH_4 inside the geologic hydrate deposits can have a significant impact on the environment. In particular, if CH_4 is released abruptly in the atmosphere, it can contribute significantly to the global warming[8,9] because CH_4 is a "greenhouse" gas that has a higher heat-trapping ability than CO_2 and, therefore, a stronger effect on the global warming problem.

Of particular industrial importance is the characteristic of hydrates to store large amounts of gas within their crystalline structure. Consequently, they have been under consideration for industrial applications of storing and transporting "energy-carrier" gases (e.g., CH_4[10−12] and H_2[13,14]).

The accurate knowledge of the storage capacity of CH_4 hydrates is a fundamental question that needs to be answered in order to utilize hydrates for industrial applications. Reliable answers can be obtained by either experimental measurements or computational calculations. Experimental approaches have been developed[15−25] and have reported the measured CH_4 content in hydrates. Circone et al.[20] reported a detailed discussion on experimental issues and difficulties that are related to measuring the gas composition of hydrates. On the other hand, grand canonical Monte Carlo (GCMC) simulations[26] (i.e., constant chemical potential, volume, and

Special Issue: In Honor of Kenneth R. Hall

Received: March 21, 2016
Accepted: July 5, 2016
Published: July 19, 2016

DOI: 10.1021/acs.jced.6b00256
J. Chem. Eng. Data 2016, 61, 2886−2896

temperature) have been considered a low-cost alternative methodology to calculate the gas content of hydrates. This methodology has been used extensively to study H_2 storage in hydrates.[27−30] The method has the important advantage of allowing the occupancy in each type of cavity, present in the hydrate structure, to be calculated separately. The application of the particular methodology to mixtures of CH_4 with other gases (e.g., CO_2) is rather straightforward. This issue is of particular interest to studies related to gas mixture separation processes. A number of studies have been reported that use MC simulations for CH_4 hydrates.[31−43]

Significant attention from industry and academia has been shown toward CH_4 hydrates resulting from their importance. Areas of primary interest include: flow assurance issues in oil/gas flow lines[44] that result from hydrate formation, the in situ formation of CH_4 hydrate in naturally occurring porous media,[45−54] and CH_4 production during hydrate dissociation within geologic formations.[55−63]

The primary focus of the current study is the calculation of the CH_4 storage capacity (i.e., CH_4 content) of structure sI hydrate, over a wide temperature (200−300 K) and pressure (0.1−220 MPa) ranges, using a MC simulation approach. We report Langmuir-type mathematical functions for the cavity occupancies, θ_i (with i = S, L, where S denotes the small cage, and L the large cage), as a function of pressure, P, and temperature, T: $\theta_i = f(P,T)$. Once such mathematical expressions for the cavity occupancies, as a function of pressure and temperature, become available, then we can calculate the CH_4 content for any given pressure and temperature. These equations can be used for the interpolation and extrapolation of the derived simulation data but also can be useful for predicting the CH_4 content in other hydrate systems (e.g., hydrates with promoters). Moreover, such analytical expressions could be used for the prediction of hydrate equilibrium (e.g., van der Waals−Platteeuw theory[64]), where the relation between occupancies and fugacity (pressure) is usually required as an input.

The particular issues that are of interest to the current study have also been examined in an earlier work,[35] where preliminary results have been reported. However, the current study provides additional new insight with regard to four different aspects, when compared to the earlier study. In particular: (i) in the current study, we use an elaborate and self-consistent approach based on MC simulations in order to relate the chemical potential and pressure of the system, whereas in the earlier study, a more crude approach was utilized that was based on the use of equations of state, (ii) in the current study, we examine a model for water that has been shown to produce more accurate calculations during molecular dynamics simulations, (iii) a more extensive comparison with experimental and computational studies is included in the current study, and finally, (iv) a discussion is provided that examines the effects of pressure on the storage capacity of naturally occurring hydrates, particularly for cases when the pressure within the deposit is significantly higher than the equilibrium pressure. This issue is of significant importance because it can affect the total amount of CH_4 present in the deposit; therefore, it can affect the discussion on the economic viability of CH_4 production from a particular hydrate deposit.

The current study is organized as follows: A brief background on hydrates and the water and CH_4 models used are initially presented. Next, we describe the simulation details. Then, the results from the MC simulations are presented, and subsequently, their comparison with available experimental data and other computational studies is discussed. Finally, a discussion on the implication to geologic media containing hydrates also is presented that is followed by the conclusions.

2. METHODOLOGY

2.1. Hydrate Structure. For the current study, the simulation box consists of 27 unit cells, (3 × 3 × 3), of sI hydrate. It contains 1242 water molecules that form a total of 54 small (5^{12}) and 162 large ($5^{12}6^2$) cavities. The space group symmetry ($Pm3n$) of the hydrate crystal has been determined from XRD measurements.[65] The atomic positions are taken from the work of Takeuchi et al.[66] and correspond to those proton configurations that have (almost) zero dipole moment among all possible configurations that obey the so-called "ice rules".[67] The lattice constant (12.03 Å) for the sI hydrate has also been taken from Takeuchi et al.[66] Furthermore, we assume that the value of the lattice constant is kept constant for the entire pressure and temperature range and water molecules are kept rigid and at fixed positions throughout the simulation. The use of a flexible water lattice would increase the computational cost.

2.2. Water and CH_4 Models. Water molecules in the current study are represented with the TIP4P/Ice[68] water model. The TIP4P/Ice is a rigid four-site model in which a LJ sphere is fixed on the oxygen site. The electrostatic contributions are implemented by positive partial charges located on each hydrogen atom and a negative partial charge fixed on an "M-site", located on the bisector of the H−O−H angle at 0.1577 Å from the oxygen atom. The O−H bond length is 0.9572 Å and the H−O−H angle is 104.52°. Values for the LJ parameters and the charges are given in Table 1. The

Table 1. Parameters of the Water Model Used in the GCMC Simulations

model	site	σ (Å)	ε (kJ/mol)	charge (e)
TIP4P/Ice[68]	O	3.1668	0.8822	0.0000
	H	0.0000	0.0000	+0.5897
	point M	0.0000	0.0000	−1.1794

TIP4P/Ice started attracting the attention of hydrate-related studies only recently, after it was initially identified as the most appropriate to predict accurately the three-phase hydrate equilibria using molecular dynamics[69] or MC simulations.[34] Subsequently, it has been used by other molecular simulation hydrate studies[37−40,70−72] as well.

Two different models are examined for the case of the CH_4 molecule. In the first model, the CH_4 molecule is represented as a single-interaction site (united−atom approach) that interacts via a 12−6 Lennard-Jones (LJ) potential. In particular, the OPLS−UA[73] model has been used for CH_4. Table 2 shows

Table 2. Parameters of the CH_4 Models Used in the GCMC Simulations

model	site	σ (Å)	ε (kJ/mol)	charge (e)	distance (Å)[a]	angle (°)[a]
OPLS−UA[73]		3.7300	1.2301	0.000	n/a	n/a
OPLS−AA[74]	C	3.500	0.27614	−0.240	d_{C-H} = 1.090	θ_{HCH} = 109.47
	H	2.500	0.12552	+0.060		

[a]n/a: not applicable.

DOI: 10.1021/acs.jced.6b00256
J. Chem. Eng. Data 2016, 61, 2886−2896

the LJ parameters for both models. The net charge of the CH_4 molecule is zero, and consequently, there are no electrostatic interactions, neither between CH_4 molecules nor between CH_4 and water. For the second model, the OPLS−AA (all−atom)[74] has been used.

2.3. Simulation Details. In the current study, we have used the GCMC methodology that was originally developed by Metropolis et al.[75] All simulations were performed with the open-source package for Monte Carlo (MC) simulations MCCCS Towhee[76] (Version 7.1.0). In the simulations, a cutoff distance of 15 Å has been used for all types of interactions. LJ interaction parameters between different types of interacting sites were calculated with the Lorentz−Berthelot combining rules.[26] No tail corrections were applied to the LJ interactions. The Ewald summation[26] was used for the long-range electrostatic interactions. In addition, 3D periodic boundary conditions were applied to the simulation box.

Each run consisted of an equilibration stage of 2×10^6 MC steps followed by a production stage of 5×10^6 MC steps. In the GCMC runs, the following MC moves were applied with equal probabilities: insertion, destruction, rotation (used only for the case of OPLS−AA), and translation. One out of every 50 steps during the production stage (10^5 steps in total) was taken into account for the average calculation of properties.

For the determination of the occupancy for each type of cavity, each CH_4 molecule was assigned to the cavity whose center was closest to the molecule's position. In this way, the average occupancy θ (i.e., average number of CH_4 molecules per cavity) can be separately calculated for every cavity type. For a hydrate structure that contains k types of cavities and there are n_i cavities of type i together with n_w water molecules in the unit cell, the gas content, expressed as weight percentage (wt %), is given by

$$(\text{wt \%}) = \frac{\mathrm{MW_g} \cdot \sum_{i=1}^{k} n_i \cdot \theta_i}{\mathrm{MW_g} \sum_{i=1}^{k} n_i \cdot \theta_i + n_w \cdot \mathrm{MW_w}} \cdot 100 \quad (1)$$

where MW_g and MW_w are the molecular weights of the guest gas and water, respectively. In the more general case where a promoter (i.e., help guest that contributes in hydrate formation under more favorable P, T conditions) is also present in the hydrate structure, the term $n_p \cdot \theta_p \cdot MW_p$ needs to be added to the denominator of eq 1, where it is assumed that the promoter has a molecular weight MW_p and occupies the cavities of type p with an average occupancy θ_p. Usually, it is assumed that all of the promoter-designated cavities are fully occupied by one promoter molecule, therefore, $\theta_p = 1$.

3. RESULTS AND DISCUSSION

3.1. Relation between Pressure and Chemical Potential of CH_4. The basic input of a GCMC run is the chemical potential of the "absorbate", which can be calculated using the Widom insertion method.[77] In order to correlate the chemical potential with the pressure we performed a series of MC simulations of bulk CH_4 in the *NVT* ensemble, namely under constant number of CH_4 molecules (N), volume (V), and temperature (T). In these *NVT* runs, a cubic simulation box was used. At every pressure value, the box volume was such that it contained at least 500 CH_4 molecules but its side length remained longer than double the cutoff distance (15 Å). In each run, the virial pressure was calculated

$$P = \frac{NkT}{V} - \frac{1}{3V} \sum_i \sum_{j>i} r_{ij} \cdot \frac{\mathrm{d}U_{ij}}{\mathrm{d}r} \quad (2)$$

The chemical potential was calculated with the Widom insertion method.[77] According to this method, after each MC step, an additional CH_4 molecule is randomly inserted in the simulation box and its potential energy U_{N+1} from the interactions with the rest of the molecules is calculated. The chemical potential μ is given by the following equation:

$$\mu = \mu_0 - kT \ln \left\langle \exp\left(-\frac{U_{N+1}}{kT}\right) \right\rangle \quad (3)$$

where $\langle \cdots \rangle$ denotes average over all MC steps, and μ_0 is the ideal gas chemical potential. The reference value of chemical potential, μ_0, is calculated from an additional *NVT* run were all interactions are set to zero. The chemical potential is calculated as a function of pressure, at constant temperature. This approach is more reliable and self-consistent than using a macroscopic equation of state (EoS), as has been done in previous studies.[28−30,35] However, it requires additional computational runs.

In this way, each run corresponds to a certain CH_4 density and for this density the pressure and chemical potential are calculated from eqs 2 and (3), respectively. This procedure not only allows the relation between pressure and chemical potential to be determined but also provides the EoS for the examined gas. This is shown in Figure 1 together with an EoS

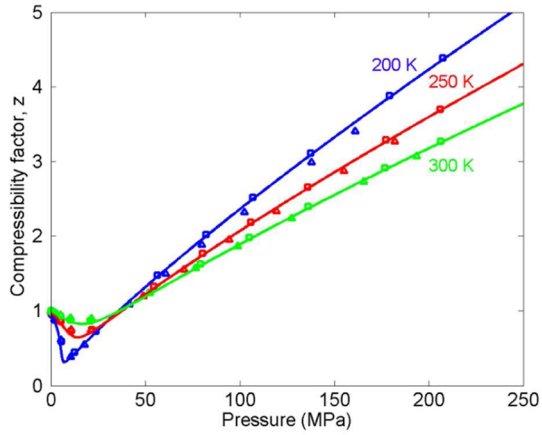

Figure 1. PVT behavior of CH_4 gas. Comparison between computational results (denoted with symbols; squares are UA, triangles are AA) obtained from *NVT* MC simulations with calculations from an experimental EoS[78] (denoted with lines). Confidence limits are smaller than the symbol sizes.

that has been directly fitted to experimental data for CH_4.[78] Even at high pressures, there is very good agreement between the MC results and the experimental EoS.

The excess chemical potential as a function of pressure is shown in Figure 2 for three temperatures. The calculated values depend on the molecular model used for CH_4. We observe that the OPLS−AA potential gives higher values than the OPLS−UA potential. However, this difference does not affect the results of the GCMC simulations since the chemical potential is converted to pressure according to the appropriate temperature-dependent curve in Figure 2. Shown also are the calculations with the accurate component-specific EoS.[78] The

DOI: 10.1021/acs.jced.6b00256
J. Chem. Eng. Data 2016, 61, 2886−2896

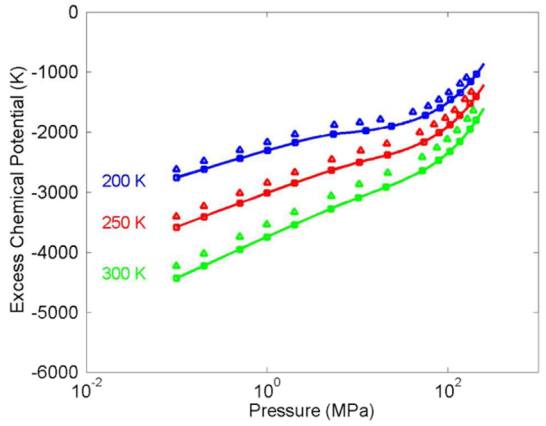

Figure 2. Excess chemical potential (μ^{ex}/k) of CH_4 gas as a function of pressure. MC data points are denoted with symbols (squares are UA, triangles are AA). Solid lines denote calculations with an experimental EoS.[78] Confidence limits are smaller than the symbol sizes.

calculations using the EoS and the OPLS−UA are in very good agreement.

3.2. Regression and Discussion of the MC Simulation Results. In the current study, we performed an extensive series of GCMC simulations for structure sI CH_4 hydrate. Simulation results are reported for the following four temperatures (isotherms): 200, 250, 270, and 300 K. The obtained MC results are reported in Tables S1−S8 of the Supporting Information, along with the confidence limits of the simulations. It is evident that due to the large number of MC realizations used for the calculation of the properties the statistical uncertainties are very low. For the particular temperatures examined, the corresponding hydrate equilibrium pressures, $P^{eq}(T)$, that are calculated using CSMGem[1] are equal to 0.117, 1.162, 2.306, and 55.507 MPa, respectively. The pressure range considered in this study includes two distinct pressure zones. One high pressure zone where the hydrate is thermodynamically stable, $[P^{eq}(T) - 220\ \text{MPa}]$, and a second low pressure zone where the hydrate is thermodynamically unstable, $[0.1\ \text{MPa} - P^{eq}(T)]$. For the second pressure zone it is essential to assume that a hypothetical CH_4 hydrate of structure sI exists and perform GCMC simulations in order to estimate the total amount of CH_4 that the hypothetical structure can absorb. Simulations at the lower pressure zone are essential only for the case of stabilizing the CH_4 hydrate using a promoter. In that case the hydrate can be stable at significantly lower pressures. One should note, however, that the use of a promoter results in lower storage capacities since a fraction of cavities is occupied by the promoter.

Figure 3a and 3b show the cavity occupancy for the small and large cages respectively, that were obtained from the GCMC simulations of the sI CH_4 hydrate, in the pressure range 0.1−220 MPa, and the considered series of isotherms. In the current study, we considered the entire pressure range for all the isotherm curves in order to be able to correlate the GCMC calculations for the cage occupancies θ_S and θ_L, using Langmuir-type curves. This is the traditional type of formulation that is used to describe the relation between cavity occupancy and fugacity or pressure.[79,80]

In particular, the GCMC results for the cage-occupancies, θ_i (with i = S, L), are fitted to the following type of curves:

$$\theta_i(P) = \frac{C_i(T)\cdot P}{1 + C_i(T)\cdot P} \tag{4}$$

where the parameter $C_i(T)$, is temperature dependent and is given by the following equation:

$$C_i(T) = \frac{A_i}{T}\cdot\exp\left(\frac{B_i}{T}\right) \tag{5}$$

Note that eq 4 is theoretically founded only for cavities that can hold one guest molecule at most (i.e., single occupancy).[1] The adjustable parameters A_i and B_i are specific to each cavity type. The obtained optimum values for the set of parameters that describe the cavity occupancies resulting from the GCMC simulations are given in Table 3.

In Figure 3, the GCMC simulation results are denoted with symbols and the lines show the Langmuir-type isotherm-fitted curves. The GCMC results and the lines that are depicted with the same color correspond to the same temperature. Very good agreement between the GCMC results and the Langmuir-type curves, fitted to the GCMC simulation results, is obtained. Furthermore, the difference between the OPLS−UA and OPLS−AA is the direct result of the difference in the excess chemical potential shown in Figure 2.

Figure 4 shows the CH_4 storage capacity (i.e., CH_4 content of the hydrate structure), expressed as wt %, of the sI hydrate as a function of pressure in the pressure range [0.1−220] MPa

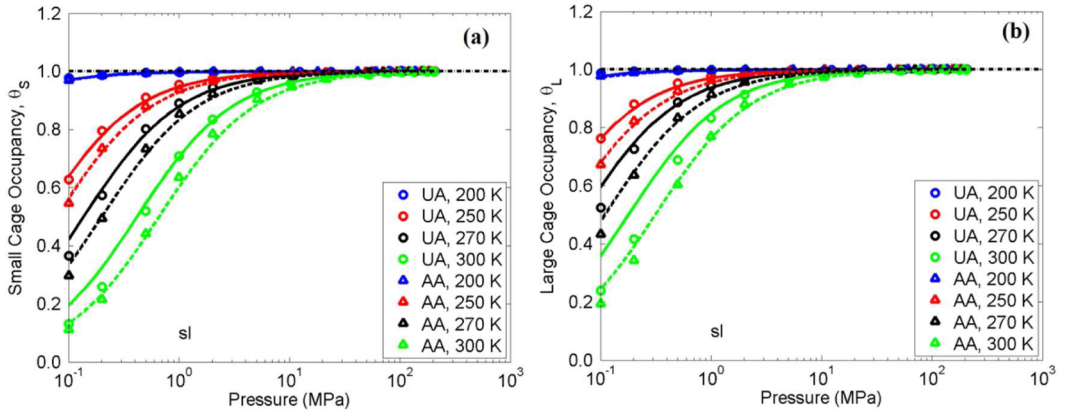

Figure 3. Cage occupancy obtained from GCMC simulations of sI CH_4 hydrate in the pressure range (0.1−220) MPa, and various isotherms for (a) the small cages and (b) the large cages. Symbols denote the GCMC results and lines (solid is UA, dashed is AA) are the Langmuir-type isotherm-fitted curves. Isotherm info depicted with the same color. Confidence limits are smaller than the symbol sizes.

DOI: 10.1021/acs.jced.6b00256
J. Chem. Eng. Data 2016, 61, 2886−2896

Table 3. Obtained Parameters for the Langmuir-Type Curves Describing the Cage Occupancies Resulting from the GCMC Simulations[a]

CH_4 model	parameter	small cavity i = S	large cavity i = L
OPLS–UA	A_i (K/MPa)	$(63.8143 \pm 15.6340) \times 10^{-3}$	$(466.5032 \pm 115.7500) \times 10^{-3}$
OPLS–UA	B_i (K)	$(27.8670 \pm 0.5233) \times 10^{2}$	$(24.3950 \pm 1.0292) \times 10^{2}$
OPLS–AA	A_i (K/MPa)	$(27.3460 \pm 3.9900) \times 10^{-3}$	$(219.2944 \pm 30.4030) \times 10^{-3}$
OPLS–AA	B_i (K)	$(29.1950 \pm 0.2404) \times 10^{2}$	$(25.2220 \pm 0.4514) \times 10^{2}$

[a]Uncertainty was estimated at the confidence level (90%).

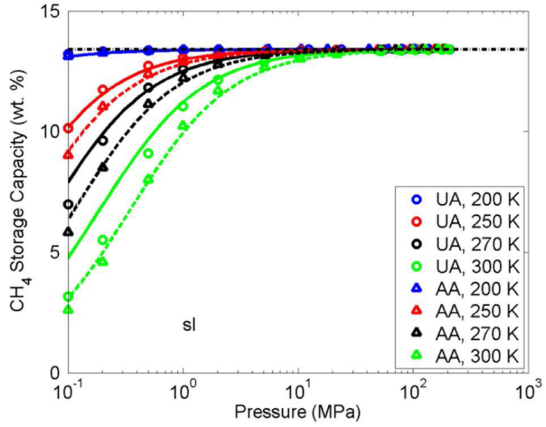

Figure 4. CH_4 storage capacity (wt %) as a function of pressure for the sI hydrate and for various isotherms. Symbols denote the GCMC simulation results and lines (solid is UA, dashed is AA) are those calculated from the Langmuir-type isotherm-fitted curves. Confidence limits are smaller than the symbol sizes.

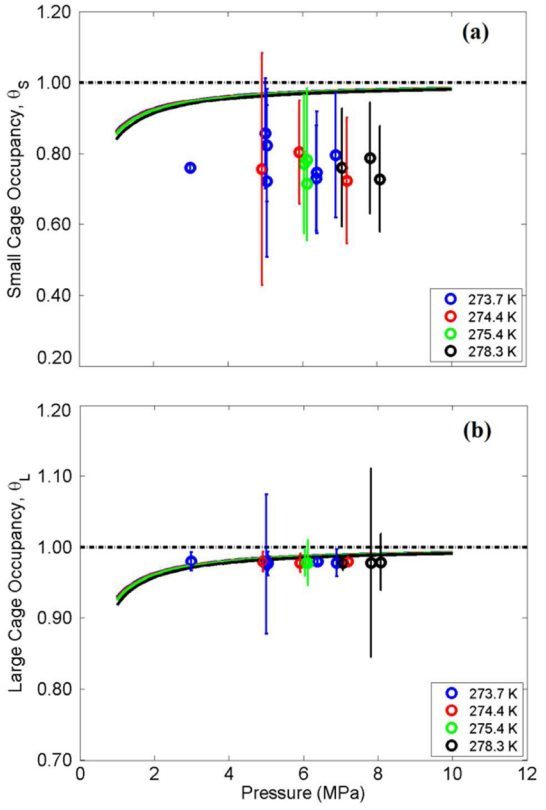

Figure 5. Cage occupancies as a function of pressure for (a) the small cages, and (b) the large cages and various temperatures. Comparison between the Langmuir-type fitted curve to the GCMC data (denoted with solid lines), and the experimental data of Uchida et al.[16] (denoted with circles).

and for the various isotherms. We examine pressures both below and above the hydrate equilibrium pressure. We observe that, for any given temperature, an increase at the pressure above the equilibrium value, results in the increase of the CH_4 content of the sI hydrate only by a limited amount. This is a direct result of the fact that the cages have already high occupancies at the hydrate equilibrium conditions. Therefore, no dramatic increase in the hydrate storage capacity can occur by increasing the pressure above the equilibrium value.

In addition, it is well known that the lattice constant of the CH_4 hydrate crystal depends on both the temperature and pressure.[25,81] However, as the MD study of Docherty et al.[81] showed, the change in the lattice constant for CH_4 hydrate at a temperature of 250 K and pressure range 3–200 MPa is approximately 0.6%. Therefore, given also that the CH_4 hydrate does not exhibit multiple cage occupancy and has also a high level of cage filling, we do not expect a significant effect of the lattice constant on the cavity occupancy results. Therefore, we consider the lattice constant fixed throughout all simulations reported in the current study.

3.3. Comparison with Experiments and Other Computational Studies. Figure 5 shows a comparison of the GCMC Langmuir-type fits with the experimental results of Uchida et al.[16] for the small and large cages. Uchida et al.[16] used Raman spectroscopy in order to measure the crystallographic hydration number, n_w, which gives the number of water molecules in the hydrate lattice per guest CH_4 molecule and is equal to $n_w = \frac{46}{6\theta_L + 2\theta_S}$. Uchida et al.[16] reported experiments in the temperature range 273.7–278.3 K, and pressure range 2.99–8.08 MPa.

Figure 5a refers to the cage occupancies for the small cages, θ_S. The experimental data are plotted versus pressure, as a series of four isotherms, where we grouped the experimental data with similar temperatures and plotted them using an average temperature (i.e., 273.7, 274.4, 275.4, and 278.3 K). Figure 5a shows also the four Langmuir-type curves using the parameters obtained in the current study by fitting the GCMC simulations (Table 3). The four curves are very close to each other and overpredict, in general, the experimental data. Note, however, that all curves fall close to the upper bound of the experimental error that was reported by Uchida et al.[16] In Figure 5b, the cage occupancies for the large cages, θ_L, are presented. For this particular case, the experimental data give an almost constant value for the large cage occupancy, $\theta_L \approx 0.98$, for all temperatures and pressures examined, implying an almost-complete cage occupancy. The GCMC Langmuir-type curves for the large cage occupancy exhibit a very good agreement with the reported experimental data.

DOI: 10.1021/acs.jced.6b00256
J. Chem. Eng. Data 2016, 61, 2886–2896

Figure 6 shows a comparison of cage occupancies as a function of pressure for isotherms in the range 268−271 K. In particular, four sets of experimental data[18,23−25] are compared with recently reported MC simulation studies[35,39,40] as well as simulations from the current study. It should be noted that Klapproth et al.[18] reported experimental data only for the small cages at 271.15 K. The experimental data of Qin and Kuhs,[23] Qin et al.,[24] and Hansen et al.[25] are at 268 K. On the other hand, the GCMC simulations that were reported by Papadimitriou et al.[35] were performed at 273.15 K, whereas the current GCMC simulations are at 270 K. Henley and Lucia[39] performed Gibbs ensemble MC (GEMC) simulations in order to calculate cage occupancies and reported values only for the total cage occupancy. They considered both a flexible and a rigid lattice. Their simulations, shown in Figure 6, correspond at a temperature equal to 270 K. Brumby et al.[40] also performed GEMC simulations at 270 K in order to calculate cage occupancies and results are shown in Figure 6. It should be noted that even though the studies are not at exactly the same temperature, the comparison is valid because within such a narrow temperature range the cage occupancies are not expected to change significantly. This behavior has been observed as well in Figure 5. The following conclusions can be reached:

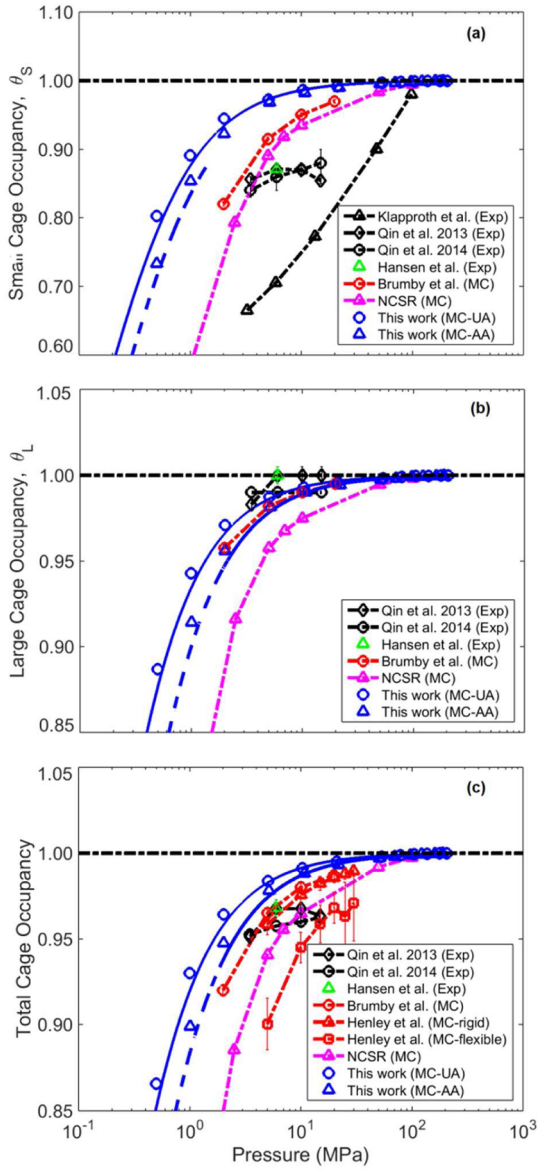

Figure 6. Cage occupancies plotted as a function of pressure for isotherms in the range 268−271 K for (a) the small cages, (b) the large cages, and (c) total cage occupancies. Blue lines (solid is UA; dashed is AA) denote the calculations using the Langmuir-type curves obtained from the current GCMC simulations. Dashed-dotted lines are guides to the eye only, connecting the corresponding experimental or earlier MC studies. NCSR denotes the GCMC simulations by Papadimitriou et al.[35] Confidence limits not shown are smaller than the symbol sizes.

- The occupancies (i.e., small, large cages) reported by the earlier study by Papadimitriou et al.[35] are lower than the current study, primarily as a result of using a smaller lattice constant in the earlier study, and secondarily as a result of using SPC/E water model in the earlier study. In a recent study on H_2 hydrates,[82] it was found that the use of SPC/E water model resulted in lower occupancies compared to the case of TIP4P/Ice.
- The GCMC simulations of the current study and those using the GEMC simulations by Henley and Lucia[39] and Brumby et al.[40] are in very good agreement with the experimental large cage occupancies (Figure 6b).
- A less satisfactory agreement is observed for the case of the small cage occupancies with the simulations, resulting in higher occupancies than the experimental values. The GCMC simulations of the current study for the case of the small cages are also higher than the GEMC simulations (Figure 6a).
- The use of a flexible lattice can result in lower cage occupancies. This is clearly shown in Figure 6c, where the simulations with a flexible lattice by Henley and Lucia[39] resulted in lower total cage occupancies when compared with simulations using a rigid lattice as the current simulations or earlier studies.[35,40]

In Figure 7, we present the cavity occupancies, as a function of temperature, for the small cavities, θ_S (Figure 7a), the large cavities, θ_L (Figure 7b), and the total cavity occupancy of the hydrate unit cell, θ_T, (Figure 7c) along the hydrate equilibrium curve $P^{eq} = f(T)$, for the sI CH_4 hydrates. Comparison is made for cavity occupancies calculated using the following three methods:

- The thermodynamic model of Sun and Duan[80]
- The commercial simulators CSMHyd[83] and CSMGem[1]
- The Langmuir-type fitted curves to the occupancy results obtained in the current study with the GCMC simulations

with reported results from MC simulations obtained by Papadimitriou et al.,[35] Jensen et al.,[34] and Ravipati and Punnathanam.[41−43] It should be noted that the simulations reported in the current study using TIP4P/Ice and the results of Papadimitriou et al. using SPC/E are based on the assumption that the three-phase P, T, equilibrium conditions are known and calculating subsequently the cage occupancies at the known conditions. On the other hand, the studies of Jensen et al.[34] and Ravipati and Punnathanam[41−43] make an effort to calculate the three-phase equilibrium conditions. Therefore, the occupancy results correspond to the equilibrium conditions that are calculated by their methodology. The error in the calculation of the equilibrium temperature results in shifting the corresponding occupancy curves by several K. A more

DOI: 10.1021/acs.jced.6b00256
J. Chem. Eng. Data 2016, 61, 2886−2896

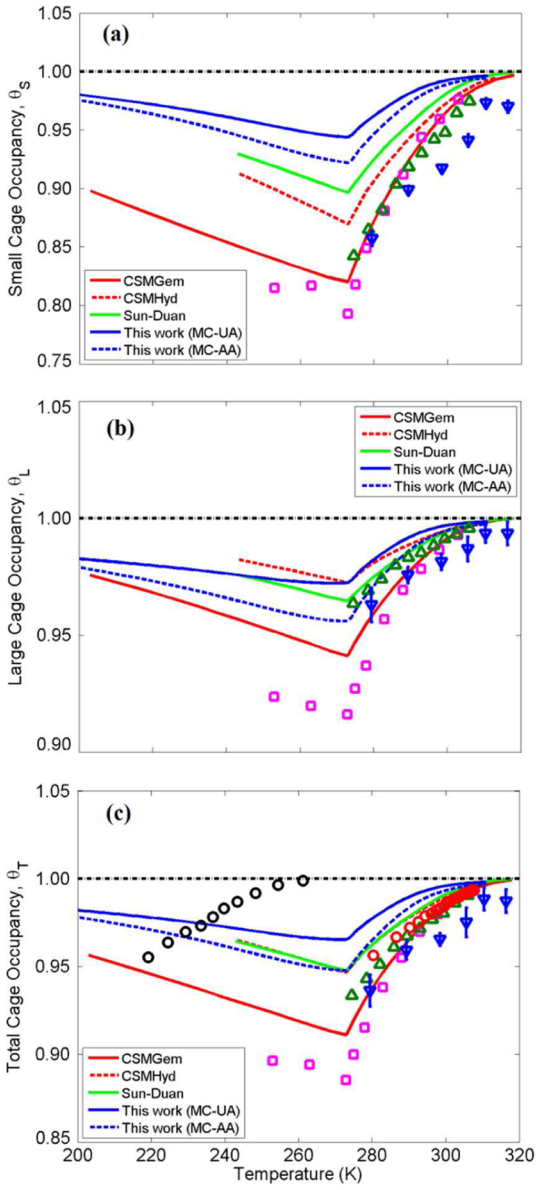

Figure 7. Calculated cage occupancies for sI CH_4 hydrates, along the hydrate equilibrium curve $P^{eq} = f(T^{eq})$ for (a) the small cages, θ_S, (b) the large cages, θ_L, and (c) the total cage occupancy, θ_T. Symbols denote MC simulations: magenta squares, Papadimitriou et al.;[35] blue triangles, Jensen et al.;[36] green triangles, Ravipati and Punnathanam;[43] circles, Ravipati and Punnathanam[43] (black is SPC/E; red is TIP4P/Ice). Confidence limits for the MC simulations of Papadimitriou et al.[35] are smaller than the symbol sizes, whereas for the experimental data of Ravipati and Punnathanam[43] are not available.

pronounced effect is observed in Figure 7c for the case of the results reported by and Ravipati and Punnathanam[43] for the SPC/E water model. We observe that the corresponding equilibrium curve is shifted considerably toward the temperature range 220−260 K. SPC/E is known to underpredict significantly the melting point of ice (i.e., it predicts a melting point of ice equal to 214 K[84]), which is reflected, as well, in the calculation of the three-phase hydrate equilibrium. On the other hand, the results reported by and Ravipati and Punnathanam[43] for the TIP4P/Ice water model, as well as, those by Jensen et al.[34] using the same model are closer to the calculations of the thermodynamic models that are considered for comparison. It should be noted that the TIP4P/Ice water model is significantly more accurate in the calculation of the melting point of ice, predicting a value equal to 270 ± 3 K.[84]

It should be noted that the models of Sun and Duan, CSMHyd, and CSMGem make use of the van der Waals−Platteeuw theory[64] coupled with an EoS. Good agreement is observed between the models of Sun and Duan and CSMHyd. A similar agreement is observed between the GCMC results of Papadimitriou et al.[35] and CSMGem. In general, CSMGem gives the lower values of all examined computational methods, whereas the current simulations with the OPLS−UA give the higher values.

Figure 8 shows a similar comparison between experimental and calculated values for the hydration number, n_w. The

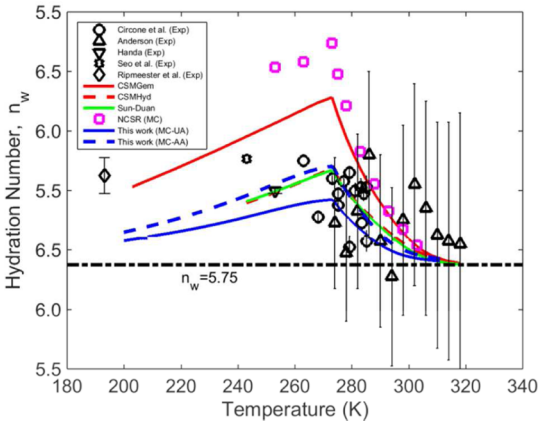

Figure 8. Hydration number, n_w, calculated using various approaches, and available experimental data for sI CH_4 hydrates along the hydrate equilibrium curve $P^{eq} = f(T^{eq})$. Confidence limits for the MC simulations of Papadimitriou et al.[35] are smaller than the symbol sizes, whereas for the experimental data of Seo et al.[19] are not available.

dashed-dotted line at the value of $n_w = 5.75$ denotes the limiting case with 100% occupancy of both small and large cages. For this particular case, the experimental data of Circone et al.[20] are used for the higher T's, whereas the experimental data of Handa[21] and Ripmeester et al.,[22] are used for the case of lower T's. Shown also are the calculations reported by Anderson,[85] which are based on the Clapeyron equation. We observe that the results from all the examined calculation methods fall within the scatter of the experimental data. The scatter of the experimental data is also an indication of the complexity and difficulty of the measurements.

Figure 9 refers to the comparison of the calculated cavity occupancy ratio, θ_L/θ_S, with the experimental data of Jager[17] for sI CH_4 hydrates. It should be noted that the experimental data of Jager[17] are within the hydrate stability zone (i.e., for a given temperature the corresponding experimental pressure is a few bars higher that the hydrate equilibrium pressure, as calculated with the correlation reported by Moridis[55]). On the other hand, all the other calculations shown in Figure 9 were performed along the hydrate equilibrium curve $P^{eq} = f(T)$. We observe that the earlier GCMC simulations reported by Papadimitriou et al.[35] are in good agreement with the experimental data of Jager for the entire temperature range. On the other hand, the current GCMC simulations exhibit good agreement only for temperatures higher than approximately 288 K.

3.4. Implication for Geological Conditions/Media.

It has been observed in various natural geologic environments (i.e., within oceanic sediments or permafrost areas) where CH_4

DOI: 10.1021/acs.jced.6b00256
J. Chem. Eng. Data 2016, 61, 2886−2896

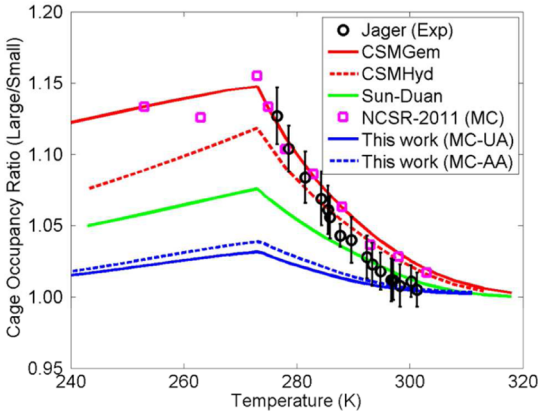

Figure 9. Calculated cage occupancy ratio, θ_L/θ_S, and experimental data for sI CH_4 hydrates reported by Jager.[17] Confidence limits for the MC simulations of Papadimitriou et al.[35] are smaller than the symbol sizes.

hydrates have been discovered that the pressure is significantly higher than the hydrate equilibrium pressure[86,87] that corresponds to the temperature of the hydrate deposit. The three-phase equilibrium conditions are calculated in the current study through the correlation reported by Moridis.[55] This behavior is clearly demonstrated in Figure 10, where the

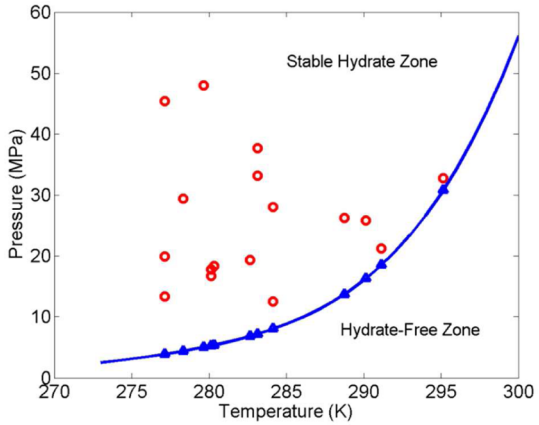

Figure 10. Prevailing P, T conditions at various oceanic sites (denoted with circles) where hydrates have been identified (Makogan et al.[86]). The solid line corresponds to the CH_4 hydrate equilibrium curve $P^{eq} = f(T^{eq})$.[55] Triangles denote the corresponding equilibrium pressures for the T conditions of the particular oceanic sites.

prevailing pressure and temperature conditions of some known oceanic hydrate sites are plotted. It is evident from the figure that certain sites have pressures that are close to the hydrate equilibrium pressure (e.g., sites Guatemala-1 and Blake Ridge-2 in ref 86, where the names are indicative of the geographic location of the hydrate deposit), whereas others can have pressures that are approximately 41.5−43.0 MPa above the hydrate equilibrium pressure (e.g., sites Nankai-2 and Peru-Chile-1 in ref 86). The following two questions were raised by Papadimitriou et al.[35] for cases where the pressure within the geological sediments is higher than the hydrate equilibrium pressure:

- "Is the amount of CH_4 enclathrated in the hydrate increased when compared to the amount at the equilibrium conditions?"
- If the answer to the previous question is yes, then "By what percent does the storage capacity increases?"

Figure 11 shows the calculation of the CH_4 storage capacity using eq 1 coupled with the Langmuir-type fits of the GCMC

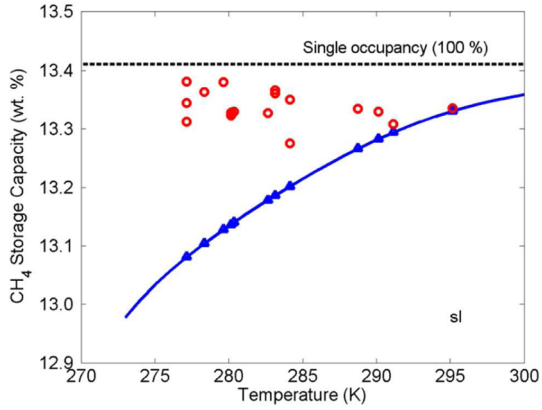

Figure 11. CH_4 storage capacity of sI hydrate (denoted with circles) calculated at the prevailing P, T conditions at various oceanic sites where hydrates have been identified (Makogan et al.[86]). The solid line corresponds to the CH_4 storage capacity at P, T conditions along the hydrate equilibrium curve $P^{eq} = f(T^{eq})$. Triangles denote the corresponding equilibrium storage capacities for the T conditions of the particular oceanic sites.

simulations for the cage occupancies. We observe a stronger effect at lower T's as a result of the lower cage occupancies at three-phase equilibrium conditions. Therefore, an increase in the pressure above the three-phase equilibrium pressure can result in an increase of the cage occupancy, approaching the limiting value of 1 (i.e., single occupancy). However, as the temperature increases, the cage occupancies (at three-phase equilibrium conditions) approach the limiting value of 1. As a result, the cage occupancies cannot increase any further, even if the pressure increases significantly. For such cases in order to obtain any additional increase in the occupancy, upon pressure increase, would require double occupancy of cages. It should be noted, however, that such behavior has not been observed for the case of sI CH_4 hydrates. Multiple occupancy for CH_4 hydrates (equal to 3.1) has been observed only for the case of large cages ($5^{12}6^8$) of sH CH_4 hydrates,[88] which are larger than the large cages ($5^{12}6^2$) of sI CH_4 hydrates.

The maximum increase in CH_4 storage capacity for the cases examined was 2.3%, corresponding to the case of Nankai-2 oceanic site. The particular value may seem insignificant at first; however, we need to keep in mind that it is applied at the field-scale of geological settings, whose size can be of the order of kilometers. Therefore, overall it could contribute a significant amount to the overall energy recovery if the hydrate deposit is large. For the particular conditions of interest, both the OPLS−UA and OPLS−AA produce similar results.

4. CONCLUSIONS

We have performed an extensive series of MC simulations on sI clathrate hydrates with CH_4 as the guest gas, over wide temperature (200−300 K) and pressure (0.1−220 MPa) ranges. It was found that the small and large cavities of sI hydrate structure cannot hold more than one CH_4 molecule, which is in good agreement with previous computational and experimental studies. Subsequently, we have developed simple

DOI: 10.1021/acs.jced.6b00256
J. Chem. Eng. Data 2016, 61, 2886−2896

equations that correlate the occupancy of each hydrate cavity with temperature and pressure. These equations are Langmuir-type and give very good correlation of the simulation results. Such expressions can be useful in hydrate-related studies (e.g., three-phase equilibrium calculations based on the van der Waals−Platteeuw theory, storage capacities) where the dependence of cavity occupancy is explicitly required as an input. An extensive comparison is performed against available experimental data and computational studies with good agreement. Finally, the developed expressions have been utilized to examine the effect of pressure on the amount of CH_4 gas that is stored in naturally occurring hydrate deposits because a number of deposits are at pressure conditions that are significantly higher than the hydrate equilibrium pressure that corresponds to the temperature of the deposit.

■ ASSOCIATED CONTENT

Supporting Information

The Supporting Information is available free of charge on the ACS Publications website at DOI: 10.1021/acs.jced.6b00256.

Values with pressure and temperature conditions where simulations were performed, the obtained MC results, and the associated confidence intervals are reported in Tables S1−S8. (PDF)

■ AUTHOR INFORMATION

Corresponding Authors

*E-mail: i.tsimpanogiannis@qatar.tamu.edu.

*E-mail: ioannis.economou@qatar.tamu.edu.

Funding

This publication was made possible thanks to an NPRP award [NPRP 6-1547-2-632] from the Qatar National Research Fund (a member of The Qatar Foundation). The statements made herein are solely the responsibility of the authors. N.I. Papadimitriou gratefully acknowledges the Greek Scholarship Foundation for the financial support under the IKY-Siemens program.

Notes

The authors declare no competing financial interest.

■ ACKNOWLEDGMENTS

We are grateful to the High Performance Computing Cluster of the Environmental Research Laboratory (NCSR "Demokritos") for generous computational resource allocation. The paper is dedicated to Professor Kenneth R. Hall, a leading figure worldwide in Chemical Engineering Thermodynamics, to honor his recent retirement from Texas A&M University at Qatar.

■ REFERENCES

(1) Sloan, E. D.; Koh, C. A. *Clathrate Hydrates of Natural Gases*, 3rd ed.; CRC Press: Boca Raton, FL, 2008.

(2) Walsh, M. R.; Hancock, S. H.; Wilson, S.; Patil, S. L.; Moridis, G. J.; Boswell, R.; Collett, T. S.; Koh, C. A.; Sloan, E. D. Preliminary report on the commercial viability of gas production from natural gas hydrates. *Energy Economics* **2009**, *31*, 815−823.

(3) Moridis, G. J.; Collett, T. S.; Boswell, R.; Kurihara, M.; Reagan, M. T.; Koh, C.; Sloan, E. D. Towards production from gas hydrates: Current status, assessment of resources, and simulation-based evaluation of technology and potential. *SPE Reservoir Eval. Eng.* **2009**, *12*, 745−771.

(4) Boswell, R.; Collett, T. S. Current perspectives on gas hydrate resources. *Energy Environ. Sci.* **2011**, *4*, 1206−1215.

(5) Milkov, A. V. Global estimates of hydrate-bound gas in marine sediments: how much is really out there? *Earth-Sci. Rev.* **2004**, *66*, 183−197.

(6) Klauda, J. B.; Sandler, S. I. Global distribution of methane hydrate in ocean sediment. *Energy Fuels* **2005**, *19*, 459−470.

(7) Pinero, E.; Marquardt, M.; Hensen, C.; Haeckel, M.; Wallmann, K. Estimation of the global inventory of methane hydrates in marine sediments using transfer functions. *Biogeosciences* **2013**, *10*, 959−975.

(8) Kvenvolden, K. A. Potential effects of gas hydrate on human welfare. *Proc. Natl. Acad. Sci. U. S. A.* **1999**, *96*, 3420−3426.

(9) Kennett, J. P.; Cannariato, G.; Hendy, I. L.; Behl, R. J. *Methane Hydrates in Quaternary Climatic Change: The Clathrate Gun Hypothesis*; American Geophysical Union: Washington, DC, 2003.

(10) Khokhar, A. A.; Gudmundsson, J. S.; Sloan, E. D. Gas storage in structure H hydrates. *Fluid Phase Equilib.* **1998**, *150−151*, 383−392.

(11) Thomas, S.; Dawe, R. A. Review of ways to transport natural gas energy from countries which do not need the gas for domestic use. *Energy* **2003**, *28*, 1461−1477.

(12) Susilo, R.; Alavi, S.; Ripmeester, J.; Englezos, P. Tuning methane content in gas hydrates via thermodynamic modelling and molecular dynamics simulation. *Fluid Phase Equilib.* **2008**, *263*, 6−17.

(13) Struzhkin, V. V.; Militzer, B.; Mao, W. L.; Mao, H. K.; Hemley, R. J. Hydrogen storage in molecular clathrates. *Chem. Rev.* **2007**, *107*, 4133−4151.

(14) Veluswamy, H. P.; Kumar, R.; Linga, P. Hydrogen storage in clathrate hydrates: Current state of the art and future directions. *Appl. Energy* **2014**, *122*, 112−132.

(15) Sum, A. K.; Burruss, R. C.; Sloan, E. D. Measurement of clathrate hydrates via Raman spectroscopy. *J. Phys. Chem. B* **1997**, *101*, 7371−7377.

(16) Uchida, T.; Hirano, T.; Ebinuma, T.; Narita, H.; Gohara, K.; Mae, S.; Matsumoto, R. Raman spectroscopic determination of hydration numbers of methane hydrates. *AIChE J.* **1999**, *45*, 2641−2645.

(17) Jager, M. D. *High pressure studies of hydrate phase inhibition using Raman spectroscopy*. Ph.D. Thesis, Colorado School of Mines, 2001.

(18) Klapproth, A.; Goreshnik, E.; Staykova, D.; Klein, H.; Kuhs, W. Structural studies of gas hydrates. *Can. J. Phys.* **2003**, *81*, 503−518.

(19) Seo, Y.-T.; Lee, H. ^{13}C NMR analysis and gas uptake measurements of pure and mixed gas hydrates: development of natural gas transport and storage method using gas hydrate. *Korean J. Chem. Eng.* **2003**, *20*, 1085−1091.

(20) Circone, S.; Kirby, S. H.; Stern, L. A. Direct measurement of methane hydrate composition along the hydrate equilibrium boundary. *J. Phys. Chem. B* **2005**, *109*, 9468−9475.

(21) Handa, Y. P. Compositions, enthalpies of dissociation, and heat capacities in the range 85 to 270 K for clathrate hydrates of methane, ethane and propane, and enthalpy of dissociation of isobutane hydrate, as determined by a heat-flow calorimeter. *J. Chem. Thermodyn.* **1986**, *18*, 915−921.

(22) Ripmeester, J. A.; Ratcliffe, C. I. Low-temperature cross-polarization/magic angle spinning ^{13}C NMR of solid methane hydrates: structure, cage occupancy, and hydration number. *J. Phys. Chem.* **1988**, *92*, 337−339.

(23) Qin, J.; Kuhs, W. F. Quantitative analysis of gas hydrates using Raman spectroscopy. *AIChE J.* **2013**, *59*, 2155−2167.

(24) Qin, J.; Hartmann, C. D.; Kuhs, W. F. Cage Occupancies of Methane Hydrates: Results from Synchrotron X-ray Diffraction and Raman Spectroscopy. *Proc. 8th Int. Conf. Gas Hydrates* (ICGH 2014); Beijing, China, **2014**.

(25) Hansen, T. C.; Falenty, A.; Kuhs, W. F. Lattice constants and expansivities of gas hydrates from 10 K up to the stability limit. *J. Chem. Phys.* **2016**, *144*, 054301.

(26) Allen, M. P.; Tildesley, D. J. *Computer Simulation of Liquids*; Oxford University Press: New York, 1987.

(27) Katsumasa, K.; Koga, K.; Tanaka, H. On the thermodynamic stability of hydrogen clathrate hydrate. *J. Chem. Phys.* **2007**, *127*, 044509.

(28) Papadimitriou, N. I.; Tsimpanogiannis, I. N.; Papaioannou, A. Th.; Stubos, A. K. Evaluation of the hydrogen-storage capacity of pure H_2 and binary H_2−THF hydrates with Monte Carlo. *J. Phys. Chem. C* **2008**, *112*, 10294−10302.
(29) Papadimitriou, N. I.; Tsimpanogiannis, I. N.; Peters, C. J.; Papaioannou, A. Th.; Stubos, A. K. 2008. Hydrogen storage in sH hydrates: A Monte Carlo study. *J. Phys. Chem. B* **2008**, *112*, 14206−14211.
(30) Papadimitriou, N. I.; Tsimpanogiannis, I. N.; Stubos, A. K. Computational approach to study hydrogen storage in clathrate hydrate. *Colloids Surf., A* **2010**, *357*, 67−73.
(31) Wierzchowski, S. J.; Monson, P. A. Calculating the phase behavior of gas-hydrate-forming systems from molecular models. *Ind. Eng. Chem. Res.* **2006**, *45*, 424−431.
(32) Wierzchowski, S. J.; Monson, P. A. Calculation of free energies and chemical potentials for gas hydrates using Monte Carlo simulations. *J. Phys. Chem. B* **2007**, *111*, 7274−7282.
(33) Sizov, V. V.; Piotrovskaya, E. M. Computer simulation of methane hydrate cage occupancy. *J. Phys. Chem. B* **2007**, *111*, 2886−2890.
(34) Jensen, L.; Thomsen, K.; von Solms, K.; Wierzchowski, S. J.; Walsh, M. R.; Koh, C. A.; Sloan, E. D.; Wu, D. T.; Sum, A. K. Calculation of liquid water-hydrate-methane vapor phase equilibria from molecular simulations. *J. Phys. Chem. B* **2010**, *114*, 5775−5782.
(35) Papadimitriou, N. I.; Tsimpanogiannis, I. N.; Stubos, A. K. Monte Carlo Simulations of Methane Hydrates. *Proc. 7th Int. Conf. Gas Hydrates* (ICGH 2011); Edinburgh, U.K., **2011**.
(36) Chakraborty, S. N.; Gelb, L. D. A Monte Carlo simulation study of methane clathrate hydrates confined in slit-shaped pores. *J. Phys. Chem. B* **2012**, *116*, 2183−2197.
(37) Lasich, M.; Mohammadi, A. H.; Bolton, K.; Vrabec, J.; Ramjugernath, D. Phase equilibria of methane clathrate hydrates from Grand Canonical Monte Carlo simulations. *Fluid Phase Equilib.* **2014**, *369*, 47−54.
(38) Lasich, M.; Mohammadi, A. H.; Bolton, K.; Vrabec, J.; Ramjugernath, D. Influence of unlike dispersion interactions in modeling methane clathrate hydrates. *Fluid Phase Equilib.* **2014**, *381*, 108−115.
(39) Henley, H.; Lucia, A. Constant pressure Gibbs ensemble Monte Carlo simulations for the prediction of structure I gas hydrate occupancy. *J. Nat. Gas Sci. Eng.* **2015**, *26*, 446−452.
(40) Brumby, P. E.; Yuhara, D.; Wu, D. T.; Sum, A. K.; Yasuoka, K. Cage occupancy of methane hydrates from Gibbs ensemble Monte Carlo simulations. *Fluid Phase Equilib.* **2016**, *413*, 242−248.
(41) Ravipati, S.; Punnathanam, S. N. Analysis of parameter values in the van der Waals and Platteeuw theory for methane hydrates using Monte Carlo molecular simulations. *Ind. Eng. Chem. Res.* **2012**, *51*, 9419−9429.
(42) Ravipati, S.; Punnathanam, S. N. Correction to "Analysis of parameter values in the van der Waals and Platteeuw theory for methane hydrates using Monte Carlo molecular simulations". *Ind. Eng. Chem. Res.* **2012**, *51*, 15796−15798.
(43) Ravipati, S.; Punnathanam, S. N. Improving the rigor and consistency of the thermodynamic theory for clathrate hydrates through incorporation of movement of water molecules of hydrate lattice. *J. Phys. Chem. C* **2015**, *119*, 12365−12377.
(44) Kelland, M. A. History of the development of low dosage hydrate inhibitors. *Energy Fuels* **2006**, *20*, 825−847.
(45) Rempel, A. W.; Buffett, B. A. Formation and accumulation of gas hydrate in porous media. *J. Geophys. Res. B* **1997**, *102*, 10151−10164.
(46) Xu, W.; Ruppel, C. Predicting the occurrence, distribution, and evolution of methane gas hydrate in porous marine sediments. *J. Geophys. Res. B* **1999**, *104*, 5081−5095.
(47) Davie, M. K.; Buffett, B. A. Sources of methane for marine gas hydrate: Inferences from a comparison of observations and numerical models. *Earth Planet. Sci. Lett.* **2003**, *206*, 51−63.
(48) Nimblett, J.; Ruppel, C. Permeability evolution during the formation of gas hydrates in marine sediments. *J. Geophys. Res. B* **2003**, *108*, 2420.
(49) Liu, X.; Flemings, P. B. Dynamic multiphase flow model of hydrate formation in marine sediments. *J. Geophys. Res.* **2007**, *112*, B03101.
(50) Babu, P.; Yee, D.; Linga, P.; Palmer, A.; Khoo, B. C.; Tan, T. S.; Rangsunvigit, P. Morphology of methane hydrate formation in porous media. *Energy Fuels* **2013**, *27*, 3364−3372.
(51) Birkedal, K.; Freeman, C. M.; Moridis, G. J.; Graue, A. Numerical predictions of experimentally observed methane hydrate dissociation and reformation in sandstone. *Energy Fuels* **2014**, *28*, 5573−5586.
(52) Mekala, P.; Babu, P.; Sangwai, J. S.; Linga, P. Formation and dissociation kinetics of methane hydrates in sweater and silica sand. *Energy Fuels* **2014**, *28*, 2708−2716.
(53) Wang, J. Q.; Zhao, J. F.; Yang, M. J.; Li, Y. H.; Liu, W. G.; Song, Y. C. Permeability of laboratory-formed porous media containing methane hydrate: observations using X-ray computed tomography and simulations with pore network models. *Fuel* **2015**, *145*, 170−179.
(54) Ruffine, L. Exploring methane-hydrate formation and dissociation in geologic materials through laboratory experiments: kinetic behavior and morphology. *Fuel* **2015**, *141*, 173−184.
(55) Moridis, G. J. Numerical studies of gas production from methane hydrates. *SPE J.* **2003**, *8*, 359−370.
(56) Moridis, G. J. Numerical studies of gas production from Class 2 and Class 3 hydrate accumulations at the Mallik Site, Mackenzie Delta, Canada. *SPE Reservoir Eval. Eng.* **2004**, *7*, 175−183.
(57) Tsimpanogiannis, I. N.; Lichtner, P. C. Parametric study of methane hydrate dissociation in oceanic sediments driven by thermal stimulation. *J. Pet. Sci. Eng.* **2007**, *56*, 165−175.
(58) Gupta, A.; Moridis, G. J.; Kneafsey, T. J.; Sloan, E. D. Modeling pure methane hydrate dissociation using a numerical simulator from a novel combination of X-ray computed tomography and macroscopic data. *Energy Fuels* **2009**, *23*, 5958−5965.
(59) Phirani, J.; Mohanty, K. K.; Hirasaki, G. J. Warm water flooding of unconfined gas hydrate reservoirs. *Energy Fuels* **2009**, *23*, 4507−4514.
(60) Myshakin, E. M.; Gaddipati, M.; Rose, K.; Anderson, B. J. Numerical simulations of depressurization-induced gas production from gas hydrate reservoirs at the Walker Ridge 313 site, northern Gulf of Mexico. *Mar. Pet. Geol.* **2012**, *34*, 169−185.
(61) Ramesh, S.; Vedachalam, N.; Ramesh, R.; Thulasiprasad, N.; Ramadass, G. A.; Atmanand, M. A. An approach for methane hydrates reservoir dissociation in a marine setting, Krishna Godhavari Basin, east coast India. *Mar. Pet. Geol.* **2014**, *58*, 540−550.
(62) Sun, Y.; Li, B.; Guo, W.; Lu, X.; Zhang, Y.; Li, K.; Wang, P.; Jin, G.; Jia, R.; Qu, L. Comparative analysis of the production trial and numerical simulations of gas production from multilayer hydrate deposits in the Qilian Mountain permafrost. *J. Nat. Gas Sci. Eng.* **2014**, *21*, 456−466.
(63) Lu, S. M. A global survey of gas hydrate development and reserves: specifically in the marine field. *Renewable Sustainable Energy Rev.* **2015**, *41*, 884−900.
(64) van der Waals, J. H.; Platteeuw, J. C. Clathrate solutions. *Adv. Chem. Phys.* **1958**, *2*, 1−57.
(65) Yousuf, M.; Qadri, S. B.; Knies, D. L.; Grabowski, K. S.; Coffin, R. B.; Pohlman, J. W. Novel results on structural investigations of natural minerals of clathrate hydrates. *Appl. Phys. A: Mater. Sci. Process.* **2004**, *78*, 925−939.
(66) Takeuchi, F.; Hiratsuka, M.; Ohmura, R.; Alavi, S.; Sum, A. K.; Yasuoka, K. Water proton configurations in structures I, II, and sH clathrate hydrate unit cells. *J. Chem. Phys.* **2013**, *138*, 124504.
(67) Bernal, J. D.; Fowler, R. H. A theory of water and ionic solution, with particular reference to hydrogen and hydroxyl ions. *J. Chem. Phys.* **1933**, *1*, 515−548.
(68) Abascal, J. L. F.; Sanz, E.; Fernandez, R. G.; Vega, C. A potential model for the study of ices and amorphous water: TIP4P/Ice. *J. Chem. Phys.* **2005**, *122*, 234511.

DOI: 10.1021/acs.jced.6b00256
J. Chem. Eng. Data 2016, 61, 2886−2896

(69) Conde, M. M.; Vega, C. Determining the three-phase coexistence line in methane hydrates using computer simulations. *J. Chem. Phys.* **2010**, *133*, 064507.
(70) Michalis, V. K.; Costandy, J.; Tsimpanogiannis, I. N.; Stubos, A. K.; Economou, I. G. Prediction of the phase equilibria of methane hydrates using the direct phase coexistence methodology. *J. Chem. Phys.* **2015**, *142*, 044501.
(71) Miguez, J. M.; Conde, M. M.; Torre, J.-P.; Blas, F. J.; Pineiro, M. M.; Vega, C. Molecular dynamics simulation of CO_2 hydrates: Prediction of three phase coexistence line. *J. Chem. Phys.* **2015**, *142*, 124505.
(72) Costandy, J.; Michalis, V. K.; Tsimpanogiannis, I. N.; Stubos, A. K.; Economou, I. G. The role of intermolecular interactions in the prediction of the phase equilibria of carbon dioxide hydrates. *J. Chem. Phys.* **2015**, *143*, 094506.
(73) Jorgensen, W. L.; Madura, J. D.; Swenson, C. J. Optimized intermolecular potential functions for liquid hydrocarbons. *J. Am. Chem. Soc.* **1984**, *106*, 6638−6646.
(74) Jorgensen, W. L.; Maxwell, D. S.; Tirado-Rives, J. Development and testing of OPLS All-Atom force field on conformational energetics and properties of organic liquid. *J. Am. Chem. Soc.* **1996**, *118*, 11225−11236.
(75) Metropolis, N.; Rosenbluth, A. W.; Rosenbluth, M. N.; Teller, A. H.; Teller, E. Equation of state calculations by fast computing machines. *J. Chem. Phys.* **1953**, *21*, 1087−1092.
(76) Martin, M. MCCCS Towhee: a tool for Monte Carlo molecular simulation. *Mol. Simul.* **2013**, *39*, 1212−1222.
(77) Widom, B. Some Topics in the Theory of Fluids. *J. Chem. Phys.* **1963**, *39*, 2808−2812.
(78) Setzmann, U.; Wagner, W. A new equation of state and tables of thermodynamic properties for methane covering the range from the melting line to 625 K at pressures up to 1000 MPa. *J. Phys. Chem. Ref. Data* **1991**, *20*, 1061−1151.
(79) Parrish, W. R.; Prausnitz, J. M. Dissociation pressures of gas hydrates formed by gas mixtures. *Ind. Eng. Chem. Process Des. Dev.* **1972**, *11*, 26−35.
(80) Sun, R.; Duan, Z. Prediction of CH_4 and CO_2 hydrate phase equilibrium and cage occupancy from ab initio intermolecular potentials. *Geochim. Cosmochim. Acta* **2005**, *69*, 4411−4424.
(81) Docherty, H.; Galindo, A.; Vega, C.; Sanz, E. A potential model for methane in water describing correctly the solubility of the gas and the properties of the methane hydrate. *J. Chem. Phys.* **2006**, *125*, 074510.
(82) Papadimitriou, N. I.; Tsimpanogiannis, I. N.; Economou, I. G.; Stubos, A. K. *Storage of H_2 in clathrate hydrates: Evaluation of different force-fields used in Monte Carlo simulations.* **2016** submitted for publication
(83) Sloan, E. D. *Clathrate Hydrates of Natural Gases*, 2nd ed.; Marcel Dekker: New York, 1998.
(84) Fernandez, R. G.; Abascal, J. L. F.; Vega, C. The melting point of ice I_h for common water models calculated from direct coexistence of the solid-liquid interface. *J. Chem. Phys.* **2006**, *124*, 144506.
(85) Anderson, G. A. Enthalpy of dissociation and hydration number of methane hydrate from the Clapeyron equation. *J. Chem. Thermodyn.* **2004**, *36*, 1119−1127.
(86) Makogan, Y. F.; Holditch, S. A.; Makogan, T. Y. Russian field illustrates gas-hydrate production. *Oil Gas J.* **2005**, *103*, 43−47.
(87) Booth, J. S.; Rowe, M. M.; Fischer, K. M. *Offshore gas hydrate sample database with an overview and preliminary analysis*: Open-File Report 96-272; U.S. Geological Survey: Reston, VA, 1996.
(88) Tulk, C. A.; Klug, D. D.; dos Santos, A. M.; Karotis, G.; Guthrie, M.; Molaison, J. J.; Pradhan, N. Cage occupancies in the high pressure structure H methane hydrate: A neutron diffraction study. *J. Chem. Phys.* **2012**, *136*, 054502.

DOI: 10.1021/acs.jced.6b00256
J. Chem. Eng. Data 2016, 61, 2886−2896

Storage of Methane in Clathrate Hydrates: Monte Carlo Simulations of sI Hydrates and Comparison with Experimental Measurements

Supporting Information

Nikolaos I. Papadimitriou[1], Ioannis N. Tsimpanogiannis[1,2,*], Ioannis G. Economou[2,*] and Athanassios K. Stubos[1]

[1] *National Center for Scientific Research "Demokritos", Environmental Research Laboratory, 15310 Aghia Paraskevi Attikis, Greece*

[2] *Texas A&M University at Qatar, Chemical Engineering Program, Education City, PO Box 23874, Doha, Qatar*

[*]Corresponding authors at: i.tsimpanogiannis@qatar.tamu.edu (Ioannis N. Tsimpanogiannis) and ioannis.economou@qatar.tamu.edu (Ioannis G. Economou)

Monte Carlo Results

Each uncertainty was estimated at the confidence limit (95%).

Table S1. OPLS – UA					Uncertainty, u	
T (K)	P (MPa)	μ/k_b (K)	θ_{Small}	θ_{Large}	θ_{Small}	θ_{Large}
200	0.100	-2752.4	0.9775	0.9870	0.0009	0.0007
200	0.200	-2614.7	0.9881	0.9934	0.0007	0.0005
200	0.502	-2434.5	0.9958	0.9973	0.0004	0.0003
200	1.010	-2301.0	0.9978	0.9986	0.0003	0.0002
200	2.038	-2173.1	0.9990	0.9993	0.0002	0.0002
200	5.391	-2027.4	0.9993	0.9997	0.0002	0.0001
200	12.374	-1971.1	0.9995	0.9998	0.0001	0.0001
200	23.711	-1896.4	0.9998	0.9998	0.0001	0.0001
200	56.300	-1716.1	0.9999	0.9999	0.0001	0.0000
200	82.010	-1594.8	1.0000	1.0000	0.0000	0.0000
200	106.861	-1456.2	1.0000	1.0000	0.0000	0.0000
200	137.455	-1339.1	1.0000	1.0000	0.0000	0.0000
200	179.156	-1156.7	1.0000	1.0000	0.0000	0.0000
200	207.510	-1032.3	1.0000	1.0000	0.0000	0.0000

Table S2. OPLS – AA					Uncertainty, u	
T (K)	P (MPa)	μ/k_b (K)	θ_{Small}	θ_{Large}	θ_{Small}	θ_{Large}
200	0.100	-2613.6	0.9688	0.9778	0.0011	0.0009
200	0.201	-2475.8	0.9854	0.9890	0.0007	0.0006
200	0.503	-2295.2	0.9942	0.9955	0.0005	0.0004
200	1.011	-2161.1	0.9970	0.9977	0.0003	0.0003
200	2.052	-2031.5	0.9983	0.9988	0.0003	0.0002
200	5.539	-1879.1	0.9994	0.9995	0.0002	0.0001
200	10.623	-1830.9	0.9994	0.9995	0.0002	0.0001
200	17.947	-1784.5	0.9995	0.9997	0.0001	0.0001
200	41.447	-1659.5	0.9997	0.9998	0.0001	0.0001
200	60.797	-1564.0	0.9998	0.9999	0.0001	0.0001
200	79.969	-1454.5	0.9999	0.9999	0.0000	0.0001
200	102.601	-1333.1	1.0000	1.0000	0.0000	0.0000
200	137.901	-1182.1	1.0000	1.0000	0.0000	0.0000
200	161.065	-1085.5	1.0000	1.0000	0.0000	0.0000

Table S3. OPLS – UA					Uncertainty, u	
T (K)	P (MPa)	μ/k_b (K)	θ_{Small}	θ_{Large}	θ_{Small}	θ_{Large}
250	0.100	-3579.3	0.6275	0.7624	0.0030	0.0026
250	0.200	-3406.7	0.7954	0.8808	0.0025	0.0020
250	0.501	-3179.5	0.9104	0.9531	0.0018	0.0013
250	1.005	-3009.4	0.9540	0.9762	0.0013	0.0009
250	2.018	-2842.6	0.9767	0.9874	0.0009	0.0007
250	5.127	-2633.6	0.9889	0.9947	0.0007	0.0005
250	10.537	-2495.6	0.9942	0.9970	0.0005	0.0003
250	21.603	-2378.0	0.9965	0.9980	0.0004	0.0003
250	54.524	-2160.5	0.9986	0.9991	0.0002	0.0002
250	80.338	-2010.4	0.9991	0.9997	0.0002	0.0001
250	105.873	-1871.7	0.9993	0.9998	0.0002	0.0001
250	135.933	-1715.6	0.9996	0.9999	0.0001	0.0001
250	177.366	-1520.9	0.9998	0.9999	0.0001	0.0001
250	205.991	-1404.3	1.0000	1.0000	0.0000	0.0000

Table S4. OPLS – AA					Uncertainty, u	
T (K)	P (MPa)	μ/k_b (K)	θ_{Small}	θ_{Large}	θ_{Small}	θ_{Large}
250	0.100	-3405.9	0.5456	0.6719	0.0031	0.0029
250	0.200	-3233.1	0.7342	0.8223	0.0027	0.0024
250	0.502	-3005.4	0.8784	0.9251	0.0020	0.0016
250	1.007	-2834.5	0.9373	0.9625	0.0015	0.0012
250	2.031	-2666.0	0.9669	0.9807	0.0011	0.0009
250	5.211	-2451.8	0.9868	0.9917	0.0007	0.0006
250	10.895	-2304.7	0.9919	0.9954	0.0006	0.0004
250	21.335	-2185.2	0.9952	0.9971	0.0004	0.0003
250	49.116	-1995.7	0.9974	0.9988	0.0003	0.0002
250	70.585	-1871.4	0.9989	0.9992	0.0002	0.0002
250	94.445	-1760.0	0.9993	0.9995	0.0002	0.0001
250	119.517	-1628.7	0.9994	0.9997	0.0002	0.0001
250	155.155	-1449.0	0.9997	0.9999	0.0001	0.0001
250	182.129	-1328.8	0.9998	0.9999	0.0001	0.0001

Table S5. OPLS – UA					Uncertainty, u	
T (K)	P (MPa)	μ/k_b (K)	θ_{Small}	θ_{Large}	θ_{Small}	θ_{Large}
270	0.100	-3917.5	0.3647	0.5252	0.0030	0.0031
270	0.200	-3730.8	0.5745	0.7265	0.0031	0.0028
270	0.501	-3485.0	0.8025	0.8868	0.0025	0.0020
270	1.004	-3300.5	0.8913	0.9428	0.0019	0.0014
270	2.015	-3118.7	0.9443	0.9709	0.0014	0.0010
270	5.097	-2887.7	0.9724	0.9874	0.0010	0.0007
270	10.374	-2727.9	0.9862	0.9930	0.0007	0.0005
270	21.155	-2584.9	0.9920	0.9960	0.0006	0.0004
270	53.688	-2345.3	0.9966	0.9983	0.0004	0.0003
270	79.143	-2186.2	0.9983	0.9990	0.0003	0.0002
270	105.497	-2043.4	0.9989	0.9995	0.0002	0.0001
270	136.936	-1884.4	0.9994	0.9997	0.0001	0.0001
270	177.535	-1697.1	0.9995	0.9998	0.0001	0.0001
270	206.554	-1546.1	0.9998	0.9999	0.0001	0.0001

Table S6. OPLS – AA					Uncertainty, u	
T (K)	P (MPa)	μ/k_b (K)	θ_{Small}	θ_{Large}	θ_{Small}	θ_{Large}
270	0.100	-3730.2	0.2961	0.4332	0.0028	0.0031
270	0.200	-3543.4	0.4926	0.6357	0.0031	0.0030
270	0.501	-3297.1	0.7330	0.8331	0.0027	0.0023
270	1.006	-3111.8	0.8533	0.9141	0.0022	0.0017
270	2.027	-2928.2	0.9225	0.9559	0.0017	0.0013
270	5.168	-2692.1	0.9680	0.9814	0.0011	0.0008
270	10.761	-2523.7	0.9819	0.9903	0.0008	0.0006
270	22.025	-2372.6	0.9899	0.9943	0.0006	0.0005
270	50.986	-2155.0	0.9956	0.9975	0.0004	0.0003
270	69.697	-2045.3	0.9966	0.9983	0.0004	0.0003
270	97.117	-1899.0	0.9980	0.9991	0.0003	0.0002
270	122.338	-1752.5	0.9989	0.9994	0.0002	0.0001
270	160.244	-1580.0	0.9995	0.9997	0.0001	0.0001
270	187.855	-1448.8	0.9997	0.9998	0.0001	0.0001

Table S7. OPLS – UA					Uncertainty, u	
T (K)	P (MPa)	μ/k_b (K)	θ_{Small}	θ_{Large}	θ_{Small}	θ_{Large}
300	0.100	-4431.6	0.1304	0.2388	0.0021	0.0026
300	0.200	-4224.1	0.2586	0.4163	0.0027	0.0031
300	0.501	-3950.3	0.5192	0.6894	0.0031	0.0029
300	1.003	-3744.4	0.7085	0.8331	0.0028	0.0023
300	2.010	-3540.4	0.8343	0.9141	0.0023	0.0017
300	5.060	-3277.6	0.9285	0.9642	0.0016	0.0012
300	10.241	-3089.0	0.9604	0.9810	0.0012	0.0008
300	20.814	-2911.8	0.9790	0.9897	0.0009	0.0006
300	52.474	-2638.0	0.9895	0.9957	0.0006	0.0004
300	79.213	-2467.6	0.9955	0.9974	0.0004	0.0003
300	105.044	-2316.2	0.9972	0.9984	0.0003	0.0002
300	136.168	-2156.2	0.9979	0.9991	0.0003	0.0002
300	176.870	-1949.4	0.9991	0.9995	0.0002	0.0001
300	206.219	-1802.1	0.9995	0.9997	0.0001	0.0001

Table S8. OPLS – AA					Uncertainty, u	
T (K)	P (MPa)	μ/k_b (K)	θ_{Small}	θ_{Large}	θ_{Small}	θ_{Large}
300	0.100	-4223.5	0.1102	0.1936	0.0019	0.0024
300	0.200	-4015.8	0.2139	0.3428	0.0025	0.0029
300	0.501	-3741.6	0.4407	0.6033	0.0031	0.0030
300	1.004	-3534.9	0.6343	0.7700	0.0030	0.0026
300	2.023	-3329.2	0.7846	0.8783	0.0025	0.0020
300	5.127	-3061.3	0.9043	0.9489	0.0018	0.0014
300	10.526	-2864.3	0.9466	0.9733	0.0014	0.0010
300	21.669	-2675.7	0.9723	0.9855	0.0010	0.0007
300	52.265	-2409.5	0.9882	0.9939	0.0007	0.0005
300	76.664	-2253.8	0.9928	0.9963	0.0005	0.0004
300	99.085	-2116.2	0.9958	0.9977	0.0004	0.0003
300	127.483	-1963.2	0.9972	0.9986	0.0003	0.0002
300	165.699	-1773.0	0.9987	0.9993	0.0002	0.0002
300	193.667	-1639.4	0.9991	0.9995	0.0002	0.0001